Nucleic Acids Research, 2006, Vol. 34, No. 3 ***785–795***
doi:10.1093/nar/gkj479

A new *anti* conformation for *N*-(deoxyguanosin-8-yl)-2-acetylaminofluorene (AAF-dG) allows Watson–Crick pairing in the *Sulfolobus solfataricus* P2 DNA polymerase IV (Dpo4)

Lihua Wang and Suse Broyde*

Biology Department, New York University, New York, NY 10003, USA

Received December 20, 2005; Revised and Accepted January 14, 2006

ABSTRACT

Primer extension studies have shown that the Y-family DNA polymerase IV (Dpo4) from *Sulfolobus solfataricus* P2 can preferentially insert C opposite *N*-(deoxyguanosin-8-yl)-2-acetylaminofluorene (AAF-dG) [F. Boudsocq, S. Iwai, F. Hanaoka and R. Woodgate (2001) *Nucleic Acids Res.*, 29, 4607–4616]. Our goal is to elucidate on a structural level how AAF-dG can be harbored in the Dpo4 active site opposite an incoming dCTP, using molecular modeling and molecular dynamics simulations, since AAF-dG prefers the *syn* glycosidic torsion. Both *anti* and *syn* conformations of the templating AAF-dG in a Dpo4 ternary complex were investigated. All four dNTPs were studied. We found that an *anti* glycosidic torsion with C1′-*exo* deoxyribose conformation allows AAF-dG to be Watson–Crick hydrogen-bonded with dCTP with modest polymerase perturbation, but other nucleotides are more distorting. The AAF is situated in the Dpo4 major groove open pocket with fluorenyl rings 3′- and acetyl 5′-directed along the modified strand, irrespective of dNTP. With AAF-dG *syn*, the fluorenyl rings are in the small minor groove pocket and the active site region is highly distorted. The *anti*-AAF-dG conformation with C1′-*exo* sugar pucker can explain the preferential incorporation of dC by Dpo4. Possible relevance of our new major groove structure for AAF-dG to other polymerases, lesion repair and solution conformations are discussed.

INTRODUCTION

The aromatic amide 2-acetylaminofluorene (AAF) and its deacetylated counterpart 2-aminofluorene (AF) are potent chemical carcinogens that have been extensively used as prototypes in mutagenesis and DNA repair studies (1,2). Upon metabolic activation, both AF and AAF selectively react with 2′-deoxyguanine (dG) to produce two predominant adducts: *N*-(deoxyguanosin-8-yl)-2-acetylaminofluorene (AAF-dG, Figure 1A) and *N*-(deoxyguanosin-8-yl)-2-aminofluorene (AF-dG) (3,4). The acetyl group causes profound differences in structural and biological properties of the two adducts. On AAF-dG, this group is too bulky to fit into the crowded region near its own sugar, when the modified guanine is in the *anti*

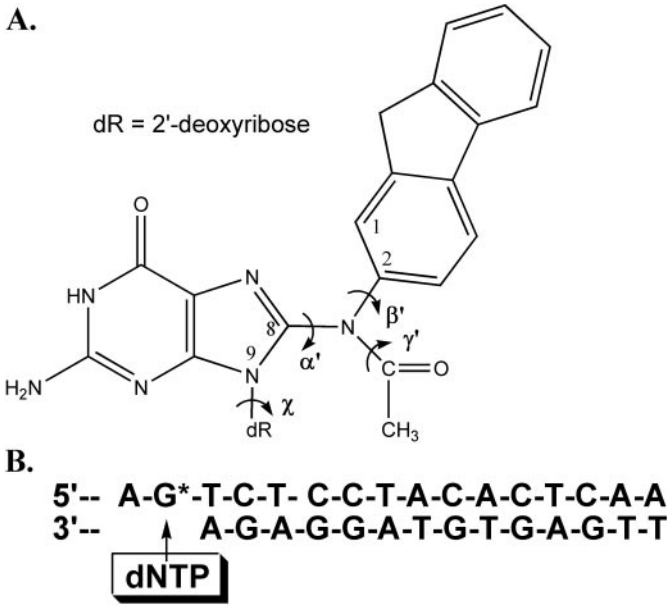

Figure 1. Structure of AAF-dG (**A**) and sequence context (**B**) for MD simulations in Dpo4. Torsion angles at the linkage site are defined as follows: α′, N9–C8–*N*–C2; β′, C8–N–C2–C1; γ′, C8–N–C–C(methyl); χ, glycosidic torsion angle O4′–C1′–N9–C4, where O4′, C1′, N9, C4 and C8 are from dG and other atoms are from AAF. G* in the sequence denotes the template guanine that pairs with an incoming nucleotide.

*To whom all correspondence should be addressed. Tel: +1 212 998 8231; Fax: +1 212 995 4015; Email: broyde@nyu.edu

domain of B-DNA. This steric problem can be alleviated by rotation of the guanine to a *syn* conformation, as first suggested in the base displacement model of Grunberger *et al*. (5), and the insertion–denaturation model of Fuchs and Daune (6,7). Proton NMR solution studies first showed on the nucleoside level that AAF-dG favors the *syn* domain while the deacetylated dG-AF favors *anti* (8). High resolution NMR solution studies have subsequently shown that the base-displaced intercalated conformation, with modified *syn* guanine displaced to the major groove and fluorenyl rings inserted into the helix, is present in a DNA duplex as ~70% of the conformational mix, with the remainder uncharacterized (9). Milhe *et al*. (10) have also noted conformational heterogeneity in AAF-dG with NMR studies. AF-dG, however, can adopt both *syn* and *anti* glycosidic torsions in B-DNA duplexes. With normal partner C opposite the lesion, the *syn* and *anti* conformers adopt base-displaced intercalated and major groove positions for the fluorenyl rings, respectively, and base-sequence context governs the population balance (11–17). Computational studies have also reflected the *syn* and *anti* conformational preferences (18–20), and the possibility of an *anti*-AAF-dG conformation was noted (19,20).

In line with these structural properties, primer extension studies (21–25) have revealed that both adducts impede DNA polymerases compared with unmodified DNA, with AAF-dG much more blocking than AF-dG, in both replicative and bypass polymerases. However, when nucleotide incorporation takes place, AAF-dG almost always strongly favors accurate incorporation of dCTP opposite the lesion (26–30), even when this dC can afterwards slip to pair with a subsequent template base (23,24,31,32). Small percentages of mismatches are also observed; the preference depends on base sequence context, nature of the polymerase and nature of the lesion. In general, dATP is the favored mismatch. In addition, mutagenesis studies have shown that AAF-dG is much more inclined to cause deletions than AF-dG when located at a site capable of forming a slipped mutagenic intermediate (23,33–38).

With the apparent requirement for the *syn* conformation in AAF-dG comes the structural problem of how dCTP is preferentially incorporated, since Watson–Crick (W/C) pairing with dG *anti* would be required in the active site of replicative DNA polymerases. While recent structural studies of bypass polymerases show several surprising templating mechanisms [e.g. Pol ι prefers Hoogsteen pairing (39,40) and Rev1 shows protein dictated templating (41)], the DNA polymerase IV (Dpo4) from *Sulfolobus solfataricus* P2 favors normal W/C pairing with the correct partner (42,43).

We have been interested in the conflict between the structural studies for AAF-dG showing the *syn* preference and polymerase studies revealing dCTP incorporation opposite the lesion. Here we investigate this problem with extensive molecular modeling and molecular dynamics (MD) simulations in a Dpo4 bypass polymerase ternary complex with all four dNTPs. Primer extension data with this polymerase (26) reveals a preference for dCTP incorporation (10% primer elongation by 1 bp) opposite AAF-dG, followed by dATP (3.6%), and dTTP (1.5%), with little dGTP (0.5%). While blocking is predominant opposite and one position prior to the lesion, some full-length extension is observed in this Dpo4 system.

We find a novel *anti* conformation for AAF-dG that easily alleviates the steric hindrance caused by the acetyl: the AAF moiety is accommodated in the major groove pocket of the Dpo4 active site with the acetyl 5′-directed and fluorenyl rings 3′-directed along the modified strand; the adducted guanine is paired with dCTP via normal W/C hydrogen bonds. The *syn* AAF-dG structures are highly distorting to the polymerase active site, regardless of the incoming dNTP. The *anti* conformation, achieved through modest adjustment of the sugar pucker from the B-DNA C2′-*endo* to the C1′-*exo* domain in the Dpo4 crystal ternary complex, might also be applicable to other polymerases. AAF-dG's capacity to adopt an *anti* conformation may also account in part for its conformational heterogeneity in solution (9,10,44), and shed light on differences between AF-dG and AAF-dG in their sequence-dependent conformational balance as well as their biological behaviors.

COMPUTATIONAL METHODS

Molecular modeling

Complex BP-2 (45) from the crystal of the Dpo4–DNA–dNTP ternary complex, with the adenine 3′ to the templating residue containing a benzo[*a*]pyrene diol epoxide adduct (PDB ID: 1S0M, chains B/E/F, and associated dNTP/ions/H_2O) (46) was employed as an initial model. In this structure the benzo[*a*]-pyrene rings were situated in the Dpo4 major groove open pocket. This structure was selected from the many available Dpo4 ternary crystals because its active site is least distorted. It has a nearly perfect coordination sphere (Figure 2, inset B) for the two divalent metal ions required for the nucleotidyl transfer reaction, contains a deoxyribose instead of an unnatural dideoxyribose at the primer 3′ end and an incoming complementary partner dNTP rather than ddNDP (42). To obtain a biologically more relevant structure, we performed the following additional remodeling: (i) the Ca^{2+} ions at the active site of the BP-2 crystal structure were replaced with Mg^{2+} ions. The extra Ca^{2+} ions trapped during crystallization were deleted; (ii) the benzo[*a*]pyrene moiety in the major groove open pocket of the polymerase was replaced with a hydrogen atom; (iii) the structure was subject to minimization and 250 ps MD equilibration upon neutralization and solvation (see MD simulation protocol); and (iv) to restore normal stacking of the guanine to which the benzo[*a*]pyrene moiety had been attached (which caused displacement of this modified guanine toward the major groove), the last snapshot from the equilibration process was obtained and the torsion angles of template residues F1904–F1907, protein residues B247, B250, B275, B293 and incoming dNTP were slightly adjusted (Supplementary Table S1). Ideal Mg^{2+} coordination distances (1.8–2.3 Å) and O3′–Pα distance of ~3.1 Å were achieved in the resulting structure. The nucleotide binding Mg^{2+} ion was chelated with Oδ2 of Asp7, Oδ2 of Asp105, O of Phe8, O2α, O2β and O1γ of the incoming nucleotide. The catalytic Mg^{2+} ion was chelated with Oδ1 of Asp7, Oδ1 of Asp105, Oε1 of Glu106, O2α of incoming nucleotide, 3′-O of the primer and the oxygen atom of a water molecule (Figure 2, inset B).

The DNA sequence was then adjusted to match that used in the primer extension reaction (Figure 1B) (26), with the dG for AAF modification situated at the templating position

opposite the incoming dCTP. This structure was used as the unmodified control. A high-resolution crystal structure of AAF (Cambridge Structural Database Refcode, ACAFLR) (47) was employed to model AAF-dG within the Dpo4 ternary complex by making a covalent bond between C8 of the templating guanine and N of the AAF moiety (Figure 1A). Linkage torsion angles α', β' and γ' (Figure 1A) were surveyed over their 360° ranges at 30° intervals in combination to locate conformations of least collision, with the glycosidic torsion of the modified guanine either *anti* ($\chi = 250.7°$) or *syn* ($\chi = 95.5°$). Four *anti*- and four *syn*-AAF-dG starting conformations were constructed (Supplementary Table S2 and Supplementary Figure S1). For the *anti*-AAF-dG conformations, a normal *anti*-dCTP, an *anti*-dATP or a *syn*-dATP was employed as the incoming nucleotide. The *syn* dATP was investigated since a Dpo4 structure with a damaged template opposite a *syn* incoming adenine has been observed previously in a crystal structure (48). For the *syn* AAF-dG, an *anti*-dCTP or an *anti*-dATP was used as the incoming nucleotide. These 20 starting systems, together with unmodified control, were subject to MD simulations, as detailed below.

Builder and biopolymer modules of InsightII 2000 (Accelrys Software, Inc.) were used for all modeling work. Molecular images were made with PyMOL (DeLano Scientific, LLC.).

MD simulation protocol

MD simulations were carried out with AMBER 8.0 (University of California, San Francisco), employing the Amber 2003 force field (49) which is an updated version of the Amber 1994 (50) and Amber 1999 (51) force fields. Each system was neutralized with 15 Na^+ ions. Counterions and hydrogen atoms of the solute (DNA, polymerase and incoming dNTP) were minimized with implicit solvent (dielc = 4.0) for 600 steps of steepest descent, followed by 600 steps of conjugate gradient. The resulting ternary complex was reoriented with SIMULAID (M. Mezei, Mount Sinai School of Medicine) to minimize the number of water molecules needed to solvate the system. A periodic TIP3P rectangular water box (52) of $\sim 100 \times 73 \times 92$ Å^3, with a buffer distance of 10 Å between each wall and the closest solute atom in each direction, was added with LEaP, totaling ~16 000 water molecules.

All systems followed the same equilibration and MD treatment: (i) minimization of the counterions and solvent molecules (except the one that participates in Mg^{2+} coordination) for 2500 steps of steepest descent and 2500 steps of conjugate gradient, with 50 kcal/mol restraints on the solute atoms; (ii) 30 ps initial MD at 10 K with 25.0 kcal/mol restraints on the solute to allow the solvent to relax; (iii) heat-up from 10 to 310 K (37°C) at constant volume over 80 ps with 10 kcal/mol restraint on the solute; (iv) 20 ps MD at constant volume and 310 K, with 10.0 kcal/mol restraints on the solute; (v) 30, 40 and 50 ps MD at 1 atm and 310 K with decreasing restraint of 10, 1 and 0.1 kcal/mol, respectively, on solute atoms, and increasing time constant of 1.0, 2.0 and 4.0 ps , respectively, for heat bath coupling for the system; (vi) production MD was conducted at 1 atm, 310 K for 3 ns.

In all MD simulations, long-range electrostatic interactions were treated with the particle mesh Ewald method (53,54). A 9 Å cutoff was applied to the non-bonded Lennard–Jones interactions. The SHAKE algorithm (55) was applied to constrain all bonds involving hydrogen atoms with relative geometrical tolerance of 10^{-5} Å. The Berendsen coupling algorithm (56) was used for temperature scaling. A 2 fs time step was used, and the translational/rotational center-of-mass motion was removed every 0.5 ps. Observation of trajectories showed no obvious overall rotation of the system; thus, energy leakage from internal motion to global rotation through the 'flying ice cube effect' (57) did not take place in these simulations.

Additional simulations for incoming *anti*-dTTP and *syn*-dGTP

For completion, one additional simulation was performed for incoming *anti*-dTTP and *syn*-dGTP, respectively, using the *anti*1 starting model (Supplementary Table S2). The choice of this starting model was dictated by results of the extensive simulations for dCTP and dATP, as detailed in Results.

Simulations for AAF modified duplex

The *Nar*I sequence CGGCG*CCAC with G* modified by AAF was investigated with a 3 ns MD simulation employing two *anti*-AAF-dG conformations acquired from the Dpo4 studies as initial models. These placed the AAF in the B-DNA major groove with W/C base pairing intact. Full details of the modeling and dynamics protocol are given in Supplementary Data.

Force field parameterization

Partial charges for each *syn*-AAF-dG starting conformation were computed with Gaussian 03 (Gaussian, Inc.) following the standard procedure (58,59), to produce a single averaged charge set for the AAF-dG residue. (The *anti* starting models were excluded from charge computation due to severe collisions caused by the acetyl group.) These charges, together with the Amber atom and topology types, are provided in Supplementary Table S3. Partial charges for dNTP's were those employed in previous work (60,61). Parameters added to the AMBER 8.0 force field for the adduct were assigned by analogy to chemically similar atom types already available in the Amber 2003 force field (49–51), and are given in Supplementary Table S3.

Trajectory analysis

Structural analyses for the trajectories were conducted with the PTRAJ and CARNAL modules of the AMBER package (University of California, San Francisco). The ANAL module of the AMBER package was employed to calculate the van der Waals interaction energy between the nascent base pair and the base pair at the primer terminus, to provide an estimate of stacking interactions.

Stability of MD simulations

Overall and lesion site structural fluctuations became reasonably stable after ~1 ns of MD simulation for all systems (Supplementary Figure S2). Therefore, the last 2 ns of the production MD were used for structural analysis. The lesion site torsion angles χ, α', β', γ' (Figure 1A) as well as the pseudorotation parameter P (62) of the linked deoxyribose

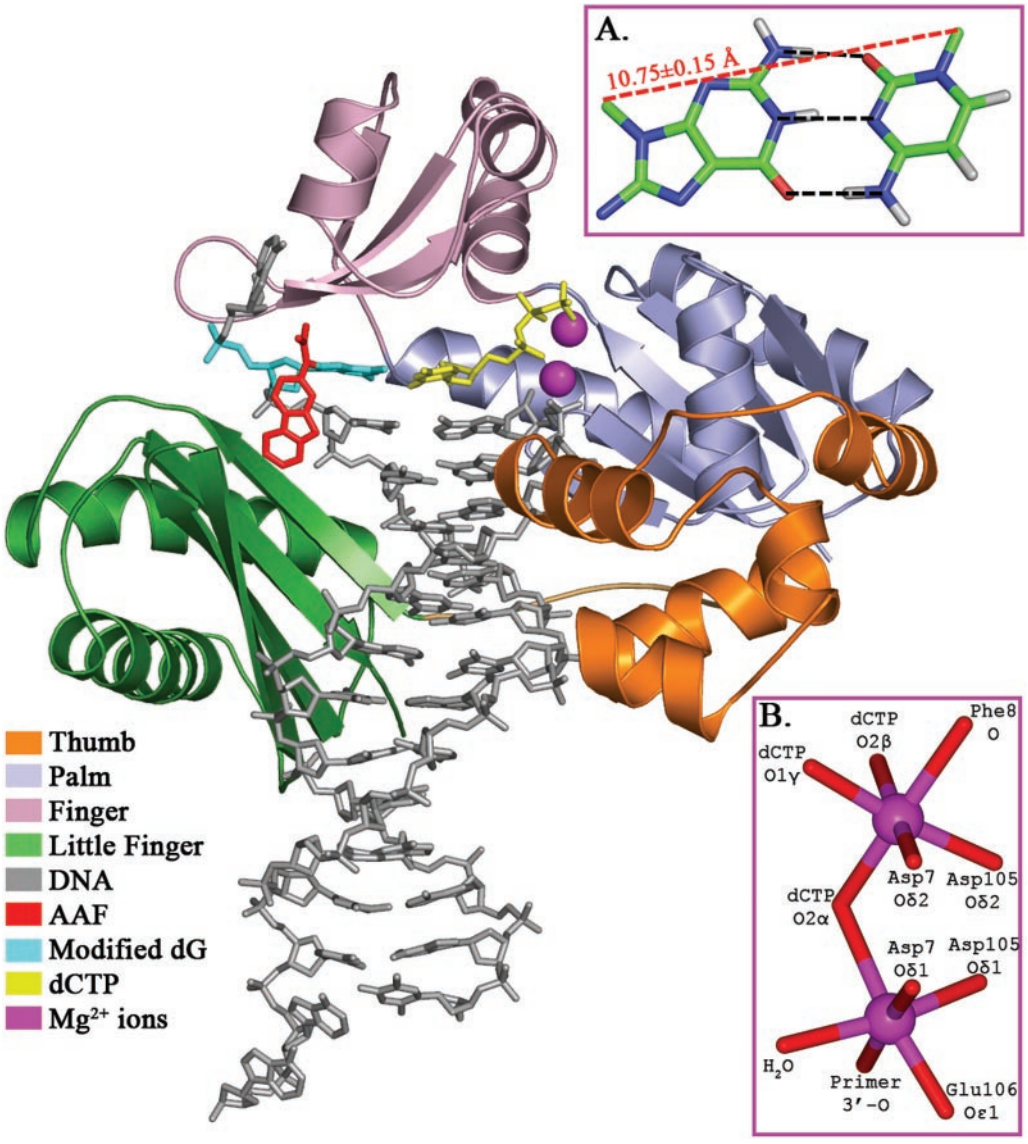

Figure 2. Stereoview of the last frame of the MD trajectory for *anti*1-AAF-dG:*anti*-dCTP at the Dpo4 active site. The polymerase is shown as cartoons; DNA strands and dCTP are shown as sticks. For clarity, hydrogen atoms are not shown. Hydrogen bonding scheme of the nascent base pair is shown in inset A. Hydrogen bonds are denoted by black dashed lines; C1′–C1′ distance is denoted by the red dashed line. Coordination spheres of the nucleotide binding and catalytic Mg^{2+} ions are shown in inset B. For illustration purpose, chelation interactions are denoted by sticks.

as function of time are shown in Supplementary Figure S3 and Supplementary Table S4.

RESULTS

We employed molecular modeling to create four *anti*- and four *syn*-AAF-dG starting conformations in the Dpo4 active site (Supplementary Table S2). These were selected to have minimal collisions and provide a representative structure for each feasible orientation of the fluorenyl rings and the acetyl group. Each *anti*-AAF-dG was investigated opposite incoming *anti*-dCTP, *anti*-dATP and *syn*-dATP. Each *syn*-AAF-dG was studied with *anti*-dCTP and *anti*-dATP. These choices were based on the near absence of *syn* pyrimidines and purine–purine mismatches with both partners *syn* in DNA structures (63). An unmodified *anti*-dG opposite an incoming *anti*-dCTP was used as control. In addition, *anti*-AAF-dG opposite *anti*-dTTP or *syn*-dGTP was investigated using results from the extensive trials with dCTP and dATP to guide selection of the starting structure. Production MD simulation was performed for 3 ns and the ensembles of structures derived from the last 2 ns trajectory were analyzed, and compared with the unmodified control simulation.

We have devised recently a customizable distortion scoring function to assess lesion impact on polymerase active site. In the present study, this function evaluates the following structural properties: (i) number of hydrogen bonds in the nascent base pair and the percent of time that the bonds are present (Supplementary Table S5 and Supplementary

Figure S7); (ii) stacking interaction between nascent base pair and base pair at the primer terminus (Supplementary Table S6 and Supplementary Figure S5); (iii) C1′–C1′ distance in the nascent base pair, normally near 10.8 Å in a W/C pair at the polymerase active site (64) (Supplementary Table S7); (iv) geometry of the dNTP binding pocket composed of '*ceiling*', '*floor*' and '*far wall*' (65) (Supplementary Figure S6); (v) distance between Pα of dNTP and O3′ of the primer terminus, with a value <3.5 Å approaching the near reaction-ready van der Waals radii sum (66) (Supplementary Table S7); (vi) angle O(primer 3′ end)–Pα(dNTP)–O3α(dNTP), ideally 180° for in-line attack of O3′ on Pα (67) (Supplementary Table S7); (vii) quality of coordination sphere of catalytic and nucleotide binding Mg^{2+} ions (Figure 2, inset B, and Supplementary Table S8); and (viii) polymerase–nascent base pair interactions (Supplementary Tables S9 and S10).

Table 1 summarizes these features for each of our simulated structures and the composite scores evaluate the structures' suitability for the nucleotidyl transfer reaction, compared with the unmodified control. While these structural criteria have been evaluated separately, there is an interdependence among them, although it is not yet clear how they are correlated to one another; it is their composite quality for a given model that provides insights. While scoring has subjective criteria elements, the scheme of Table 1 represents the current stage in our ongoing effort to evaluate polymerase active site distortions.

Unmodified control

In the unmodified control simulation, the ternary complex contained an unmodified templating guanine W/C paired with incoming dCTP. Stereoviews of the ternary complex structure, active site base stacking and dNTP binding pocket geometry at the end of the 3 ns simulation are shown in Panel A of Supplementary Figures S4–S6. We found that the structural features critical to catalysis were maintained throughout the course of the simulation. The W/C hydrogen bonds in the nascent base pair were highly occupied (>99% of the time) (Supplementary Table S5 and Supplementary Figure S7A). The base pair stacking (Supplementary Figure S5A), C1′–C1′ distance (10.75 ± 0.15 Å and 100% occupancy, Supplementary Table S7), the dNTP binding pocket geometry (Supplementary Figure S6A), and coordination spheres of the two active site Mg^{2+} ions (Supplementary Table S8) are normal. The Pα–O3′ distance is 3.19 ± 0.17 Å, with 96.95% occupancy of the near-reaction-ready distance (⩽∼3.5 Å), and the in-line attack angle is 167.08 ± 5.12° (90.90% occupancy of the 170 ± 10° range for the nucleotidyl transfer reaction, Supplementary Table S7). Polymerase residues Tyr10/Lys159 in the palm domain, Phe11/Try12/Ser34/Thr45/Tyr48/Arg51 in the finger domain and Thr250/Arg331 in the littler finger domain form hydrogen bonds with the nascent base pair (Supplementary Tables S9 and S10). The phenyl ring of Tyr12 also stacks with the sugar ring of the dCTP throughout the simulation.

Table 1. Composite evaluation of active site distortion in the Dpo4 ternary complexes compared to unmodified control

dNTP	AAF-dG	HB geometry[a]	Stacking[b]	C1′–C1′ distance[c]	Pocket geometry[d]	Pα–O3′ distance[e]	Mg^{2+} coordination[f]	In-line attack[g]	Protein interaction[h]	Composite score	Group average
Control		0	0	0	0	0	0	0	0	0	0
anti-dCTP	*anti*1	0	0	0	0	0	−1	0	0	−1	−2
	*anti*2	0	−1	0	0	0	−1	0	−2	−4	
	*anti*3	0	0	0	0	0	−1	0	0	−1	
	*anti*4	0	0	0	0	0	−1	0	−1	−2	
	*syn*1	−3	−2	−2	−1	0	−1	0	−2	−11	−9.5
	*syn*2	−2	−1	−2	−1	0	0	0	−1	−7	
	*syn*3	−3	−1	−2	−2	0	−1	0	−3	−12	
	*syn*4	−3	−1	0	−2	0	−1	0	−1	−8	
anti-dATP	*anti*1	−1	−1	−2	0	−1	−1	0	−2	−8	−7
	*anti*2	−1	−1	−2	0	−1	−1	0	−1	−7	
	*anti*3	−1	−1	−2	0	−1	−1	0	−1	−7	
	*anti*4	−1	−1	−2	0	0	−1	0	−1	−6	
	*syn*1	−3	−1	−2	−1	0	−1	0	−3	−11	−10.3
	*syn*2	−3	0	0	−1	−2	−1	0	−2	−9	
	*syn*3	−3	−2	0	−1	0	−1	0	−3	−10	
	*syn*4	−3	−1	−2	−1	−1	−1	0	−2	−11	
syn-dATP	*anti*1	−1	0	0	0	0	−1	0	−1	−3	−4.8
	*anti*2	−2	0	0	0	0	−1	0	−3	−6	
	*anti*3	−1	0	0	0	0	−1	0	−3	−5	
	*anti*4	−1	0	0	0	0	−1	0	−3	−5	
anti-dTTP	*anti*1	−1	0	0	0	0	−1	0	−2	−4	−4
syn-dGTP	*anti*1	−2	−1	−2	0	0	0	0	−1	−6	−6

[a]0, three hydrogen bonds of ⩾90% occupancy; −1, only two hydrogen bonds of >90% occupancy; −2, only one hydrogen bond of ⩾90% occupancy or two hydrogen bonds of ⩾50% occupancy; −3, no hydrogen bonds of ⩾90% occupancy. For details see Supplementary Table S5 and Supplementary Figure S7.
[b]0, normal stacking between the nascent base pair and adjacent pair; −1, partial stacking; −2, no stacking. For details see Supplementary Figure S5.
[c]0, occupancy ⩾90%; −1, 10% ⩽ occupancy < 90%; −2, occupancy <10%. For details see Supplementary Table S7.
[d]0, none of the three walls is significantly distorted; −1, one wall is distorted; −2, at least two walls are distorted. For details see Supplementary Figure S6.
[e]0, occupancy ⩾90%; −1, 50% ⩽ occupancy < 90%; −2, occupancy <50%. For details see Supplementary Table S7.
[f]0, occupancy ⩾50% for all chelation interactions; −1, occupancy ⩾50% for all but one chelation interactions. For details see Supplementary Table S8.
[g]0, occupancy ⩾50%; −1, occupancy <50%. For details see Supplementary Table S7.
[h]Total loss of interactions between the template/dNTP and 1, 2 or ⩾3 protein residues penalizes the score by 1, 2 or 3, respectively. For details see Supplementary Tables S9 and S10.

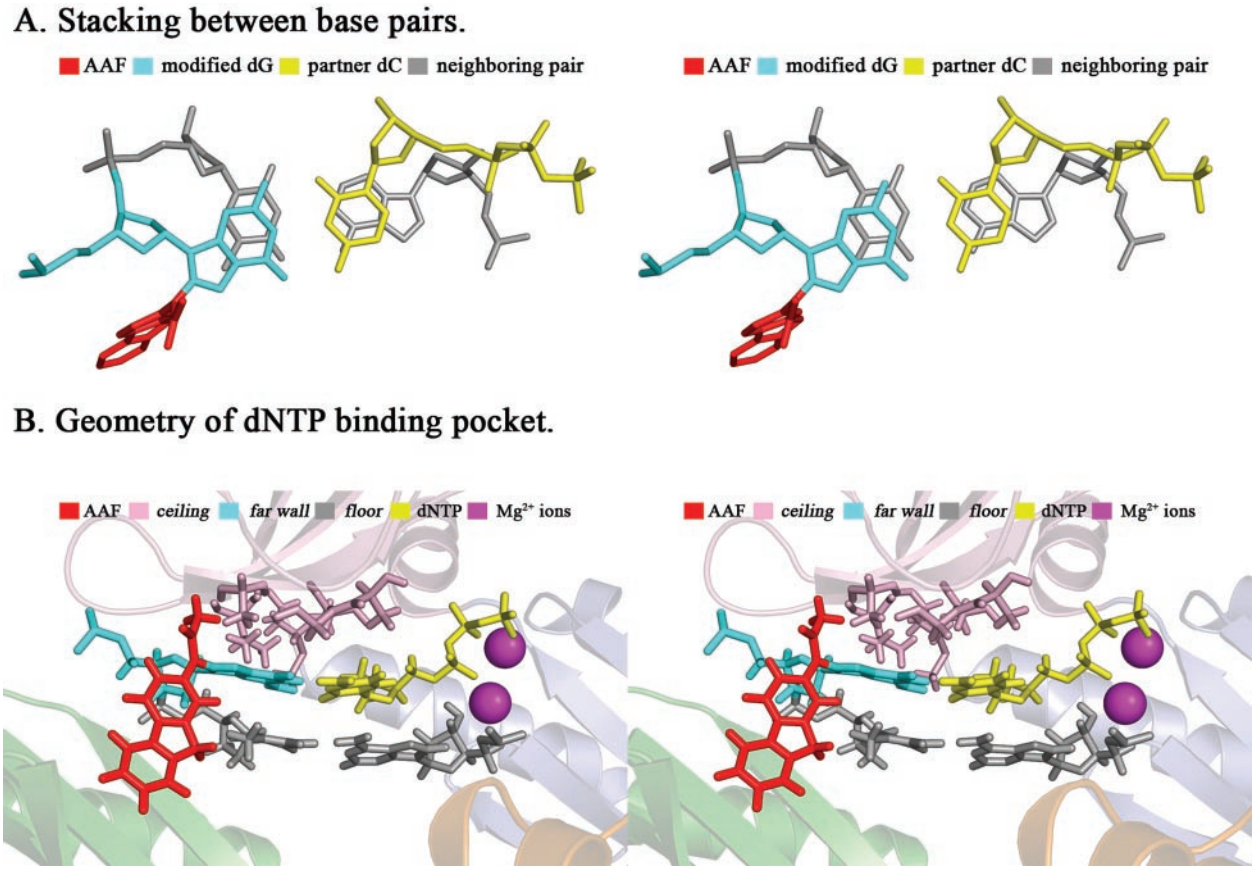

Figure 3. Stereoviews of stacking interactions (**A**) and the dNTP binding pocket geometry (**B**) from the last frame of the MD trajectory for *anti*1-AAF-dG:*anti*-dCTP at the Dpo4 active site. The polymerase is shown in transparent cartoons, using the same color code as in Figure 2. The dNTP binding pocket for our system is defined as follows: *ceiling*, Val32/Ala42/Ala44/Ala47/Gly58/Met76 in the Dpo4 finger domain; *floor*, the neighboring base pair of the nascent pair; *far wall*, the template guanine base.

anti-AAF-dG opposite *anti*-dCTP, *anti*-dATP or *syn*-dATP

The presence of major and minor groove pockets at the active site of Dpo4 allows for the accommodation of a bulky adduct on either side of the primer–template complex (42). We modeled AAF-dG in both *anti* and *syn* conformations to determine the preferred conformation of this adduct within Dpo4. With AAF-dG *anti*, the fluorenyl rings are in the major groove pocket, while they are on the minor groove side when AAF-dG is *syn*. The collisions between the acetyl and the sugar ring in our *anti* starting models were relieved during the course of the simulations. With the single exception of *anti*4-AAF-dG opposite *anti*-dCTP (Supplementary Figure S6E), all other *anti*-AAF-dG starting models (opposite incoming *anti*-dCTP, *anti*-dATP or *syn*-dATP) converged to a family of conformations with the acetyl group oriented toward the 5′-direction and the fluorenyl moiety toward the 3′-direction of the template strand. A snapshot of the last frame for *anti*1-AAF-dG opposite *anti*-dCTP, shown in Figures 2 and 3, is representative. The family members differed somewhat in local orientation of the fluorenyl rings and acetyl conformation (Supplementary Table S4 and Panels B–E, J–M and R–U of Supplementary Figure S3). The one structure with 5′-oriented fluorenyl rings, *anti*4-AAF-dG opposite *anti*-dCTP, is stabilized by stacking of the fluorene with the unpartnered base on the 5′ side of AAF-dG. Stereoviews of ternary complex structures, base stacking and dNTP binding pocket geometry of the active sites after 3 ns MD simulation are shown in Panels B–E, J–M and R–U of Supplementary Figures S4–S6. The AAF-dG in all these structures (except the *anti*4-AAF-dG:*anti*-dCTP case) adopted an *anti* conformation where the sugar pucker became C1′-*exo*, a small shift from the C2′-*endo* conformation more common in B-DNA (68). The change in the sugar pucker from C2′-*endo* to C1′-*exo* relieves the steric hindrance between the AAF and the sugar C5′ methylene when the modified guanine is *anti*, as illustrated in Figure 4. A moderate decrease in glycosidic torsion angle χ (by $\sim 20^{\circ}$ compared with control) accompanies this repuckering (Supplementary Table S4).

Significant differences were observed with different incoming dNTPs (Supplementary Tables S5–S10, Panels B–E, J–M and R–U of Supplementary Figures S4–S6 and Panels B–M of Supplementary Figure S7). With an incoming *anti*-dCTP, structural characteristics of the active site were largely comparable with those of the unmodified control. With an incoming *anti*-dATP, two hydrogen bonds with high occupancy are formed in the nascent base pair of each system, but the widths of the nascent base pairs are >12.7 Å, resulting in worsened Pα–O3′ distances and Mg^{2+} coordination spheres. With an incoming *syn*-dATP, two stable hydrogen bonds are formed

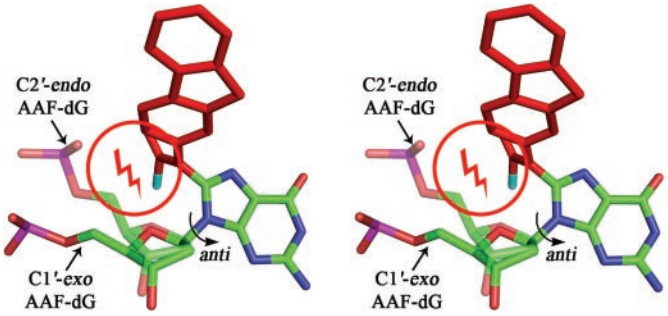

Figure 4. Stereoview of C2′-*endo* and C1′-*exo* AAF-dG structures, superimposed on the base and AAF moiety. The C1′-*exo* AAF-dG is taken from the last snapshot of the *anti*1-AAF-dG:*anti*-dCTP trajectory ($P = 120.4°$). The C2′-*endo* AAF-dG ($P = 162.0°$) differs from the C1′-*exo* AAF-dG only in the sugar pucker pseudorotation angle, P (62,80). Other torsions are $\chi = 201.8°$, $\alpha' = 101.0°$, $\beta' = 30.7°$ and $\gamma' = 33.6°$. The nucleotides are colored by atom with the AAF moiety shown in red and the methyl of the acetyl group in cyan. For clarity hydrogen atoms are not shown. Collision is denoted by the red circle.

in the nascent base pairs, with C1′–C1′ distance between 11.0 and 11.5 Å, only modestly higher than the control value of 10.8 Å. The dNTP binding pocket geometry and the Pα–O3′ distance were not significantly different from the unmodified control.

syn-AAF-dG opposite *anti*-dCTP or *anti*-dATP

The preferred base-displaced intercalated conformation of AAF-dG in a DNA duplex (9) is characterized by *syn* guanine displaced to the major groove of the helix, with fluorenyl rings intercalated, in place of the extruded guanine. However, in such a conformer the fluorenyl rings would occupy the position of the incoming dNTP within the polymerase, which would be blocking. To determine whether a *syn*-AAF-dG structure which can accommodate an incoming dNTP is feasible in the polymerase, the four *syn*-AAF-dG starting conformations (Supplementary Table S2), each opposite an *anti*-dCTP or *anti*-dATP, were subject to MD simulations. We found that the accommodation of AAF in the minor groove pocket completely impairs the capability for selecting a complementary dNTP via guanine's Hoogsteen edge. Only one weak or no hydrogen bond can be formed between AAF-dG and the incoming nucleotide, with mediocre occupancy (Supplementary Table S5). At least one wall of the dNTP binding pocket in each case is greatly distorted (Panels F–I and N–Q of Supplementary Figure S6). Owing to the bulk and non-planarity of the acetyl group (methyl and carbonyl), stacking between the nascent base pair and the adjacent one is also notably penalized or completely abolished, resulting in shearing or buckling of bases (Panels F–I and N–Q of Supplementary Figure S5), and significantly higher stacking energy in comparison with their respective *anti*-AAF-dG counterparts (Supplementary Table S6). C1′–C1′ and Pα–O3′ distances, and protein–nascent base pair interactions are adversely affected to variable extents (Supplementary Tables S7–S10).

*anti*1-AAF-dG opposite *anti*-dTTP or *syn*-dGTP

Owing to the large number of simulations, we conducted a 3 ns MD simulation only for a representative *anti* starting conformation (*anti*1-AAF-dG, Supplementary Table S2) opposite an incoming *anti*-dTTP or *syn*-dGTP. The *syn*-AAF-dG starting conformations were eliminated at this stage because the extensive simulations for dCTP and dATP showed poor accommodation of *syn*-AAF-dG at the polymerase active site, irrespective of the incoming nucleotide. The exclusion of *syn*-dTTP and *anti*-dGTP was based on the virtual absence of *syn* pyrimidines and *anti*-G:*anti*-G pair in the Nucleic Acid Database (63). AAF-dG formed a wobble pair with dT (Supplementary Table S5 and Supplementary Figure S7N), without greatly distorting the active site. With *syn*-dGTP, however, the C1′–C1′ distance reached a huge ~13.5 Å, with a bifurcated hydrogen bond in the nascent base pair (Supplementary Table S7 and Supplementary Figure S7O).

Summary of results

anti-AAF-dG can be accommodated at the Dpo4 active site via a C1′-*exo* puckered sugar conformation, with the acetyl group oriented 5′, and the fluorenyl rings directed 3′ to the modified base. The *syn*-AAF-dG, though preferred in duplex DNA, distorts the Dpo4 active site much more severely than *anti*-AAF-dG, whether or not a mismatch is involved. Not only is *syn*-AAF-dG poorly accommodated, it is also incapable of selecting and stabilizing a dCTP via its Hoogsteen edge due to the adducted bulk on guanine C8. Of the cases investigated, an incoming *anti*-dCTP is best accommodated opposite *anti*-AAF-dG, while dGTP is accommodated least well, even though it adopts the *syn* conformation.

DISCUSSION

anti-AAF-dG conformation

Structure–function relationships in AAF-dG modified DNA have been studied for many decades, but an important puzzle has not yet been resolved: how does the adduct allow preferential incorporation of dCTP within a DNA polymerase, specifically Dpo4 in the present study, while the AAF-dG strongly favors the *syn* glycosidic conformation which precludes W/C base pairing in B-DNA? In the present work we have investigated this problem in the model Y-family DNA polymerase Dpo4, for which primer extension data show dNTP incorporation preference dC > dA > dT > dG, with significant blockage one base prior to and opposite the lesion.

Our extensive modeling and MD simulations have uncovered a new structure for AAF-dG which alleviates the steric hindrance between the acetyl group and the sugar linked to the AAF-dG. A modest change in the sugar pucker from the normal B-DNA C2′-*endo* to C1′-*exo* when the AAF-dG is *anti*, as shown in Figure 4, relieves the collisions. This simple conformational adjustment solves the steric problem for the *anti* conformation directly on the nucleoside level where it originates, and it is feasible irrespective of the incoming dNTP in our simulations. Possibly this facile conformational adjustment is achievable in other polymerases where dCTP incorporation is observed opposite AAF-dG (27–30).

This conformation in Dpo4 places the fluorenyl rings in the major groove open pocket of the polymerase, with the acetyl group directed 5′ along the modified strand and the fluorene 3′-oriented. All but 1 of the 14 *anti*-AAF-dG simulations converged to this family. The non-converging structure contains

anti-AAF-dG and the fluorenyl rings stacked with the next-to-be-replicated base, which would prevent its subsequent entry into the active site (Supplementary Figure S4E). Other conformers are not suitable for nucleotide incorporation. These include all *syn*-AAF-dG conformers, which either seriously distort the polymerase active site when the fluorenyl moiety is in the small minor groove pocket, or prevent dNTP entry when the fluorenyl rings are stacked with the first base pair in the duplex region.

Replication blockage by AAF-dG

In replicative polymerases, AAF-dG is highly blocking (21,22,24,32). Crystal structures of this adduct in T7 (69) and BF (21) polymerases show that the adduct either prevents dNTP entry (T7), or prevents the modified template from entering the preinsertion site (BF). The AAF-dG is *syn* in T7, while in BF its coordinates could not be resolved due to partial disorder. Blockage by lesions in replicative polymerases *in vivo* is currently understood to cause polymerase switch, with recruitment of one or more bypass polymerases for translesion synthesis (70). These polymerases have much lower fidelity than the replicative ones, and lesion-induced mutations are currently believed to occur largely through such error-prone bypass (71). In the case of Dpo4, while normal partner dC incorporation is preferred opposite AAF-dG, mismatches are also obtained, with dA favored over dT and dG (26). Our results suggest that the observed incorporation preference in Dpo4 may have arisen from the requirement by the polymerase for AAF-dG to adopt an *anti* conformation opposite dNTP at the active site, with *anti*-dCTP least distorting, *syn*-dGTP most perturbing, and *anti*-dTTP and *syn*-dATP intermediate (Table 1). However, we appreciate that uncertainties in both the data itself and our scoring for the simulations mandate caution in comparing them.

The data of Boudsocq *et al*. (26) showed that replication is much more severely impeded for the AAF-modified DNA than for the unmodified one. Blockage opposite and one base prior to the lesion is the predominant effect. While our scoring function shows that incorporation of dCTP opposite the *anti*-AAF-dG is only slightly distorting compared with the unmodified control (Table 1), it does not evaluate potential hindrance to polymerase translocation and to template/dNTP entry into the active site. The observed blockage may stem from a number of difficulties that the polymerase encounters in the face of the adduct. As we have found, the preferred *syn*-AAF-dG conformation is highly distorting at the Dpo4 active site, which would inhibit the nucleotidyl transfer reaction, with replication aborted one base prior to the lesion. Our *anti* conformation allows AAF-dG to enter the active site, pair with an incoming dNTP which can then react with the primer 3′ terminus; however, further extension past the lesion may be inhibited due to placement of the AAF bulk in the vicinity of the little finger domain, which facilitates translocation (72). A two-step translocation mechanism (73) has been deduced recently from crystal structures of binary and ternary complexes of Dpo4: it entails movement first of the little finger during nucleotide binding, followed by thumb movement during chemical reaction. The replication cycle involves a screw-like counterclockwise rotation/translation of the polymerase along the DNA long helix when viewed in the 5′–3′ direction of the template strand. This threading of the DNA through the polymerase places the next templating base in the active site, awaiting entry of its complementary dNTP. Our predominant *anti* AAF-dG structure in Dpo4 appears to impede this translocation mechanism: upon binding of dNTP opposite *anti*-AAF-dG, translocation of the thumb domain may proceed normally, completing the chemical reaction and bringing the next template base (5′ to AAF-dG) into the active site. However, the subsequent translocation of the little finger domain is impeded since the fluorenyl rings are positioned to collide with the rotating little finger (Figure 2), hence preventing incorporation of the partner dNTP of the template base 5′ to AAF-dG.

In order to achieve further extension, as observed to a very small extent (26), repositioning of AAF-dG would be required. One possibility might involve looping out of the AAF-dG residue towards the minor groove gap between the little finger and finger domains. Ling *et al*. (72) have observed such looping out of an abasic site in Dpo4. If the loop is maintained, a deletion would result. Alternatively, the loop may realign once the polymerase has transited the adduct; depending on sequence, this dislocation mechanism could produce a mismatch mutation (74). As pointed out by one of the reviewers, the significant structural changes involved in the movement of the AAF moiety from the developing major groove to the developing minor groove may require that the DNA dissociate from the polymerase, rearrange and reassociate prior to extension.

Conformational heterogeneity of AAF-dG

The *anti* AAF-dG structure also provides insights on differences in biological properties between AF-dG and AAF-dG adducts. In DNA polymerases, AAF-dG is much more blocking in primer extension studies. In addition, AAF-dG is excised by the human nucleotide excision repair machinery much more efficiently than AF-dG (75). From a structural perspective, AAF's much greater tendency to adopt the abnormal *syn* conformation can account for these observations. However, our *anti* structure provides a subtle further understanding. AF-dG has been known for some time to manifest a sequence-governed equilibrium between *anti* major groove conformations and *syn* base-displaced intercalated ones (11–17), while for AAF-dG only a *syn* base-displaced intercalated conformation has been characterized (9). However, our *anti* conformation suggests the possibility for such an equilibrium in AAF-dG, although likely more shifted toward *syn*. We have employed a 3 ns MD simulation (see Methods and Supplementary Data) to obtain such a model in a DNA duplex based on two structures (*anti*1-AAF-dG:*anti*-dCTP and *anti*3-AAF-dG:*anti*-dCTP) from the polymerase simulations. Notably, the two conformations in the polymerase converged to the same final structure in duplex DNA (Figure 5). The C1′-*exo* conformation of the AAF-dG sugar remains stable in this major groove model and the W/C pairing remains intact. It should be noted that C1′-*exo* ($P \approx 120\,^{\circ}$) is observed as a less predominant conformation in B-DNA (68,76,77), apparently stabilized in certain sequence contexts. Other *anti*-AAF-dG conformations, coupled with specific sugar puckers (e.g. O4′-*endo* as observed in the *anti*4-AAF-dG:*anti*-dCTP simulation, Supplementary Table S4 and Supplementary Figure S6E),

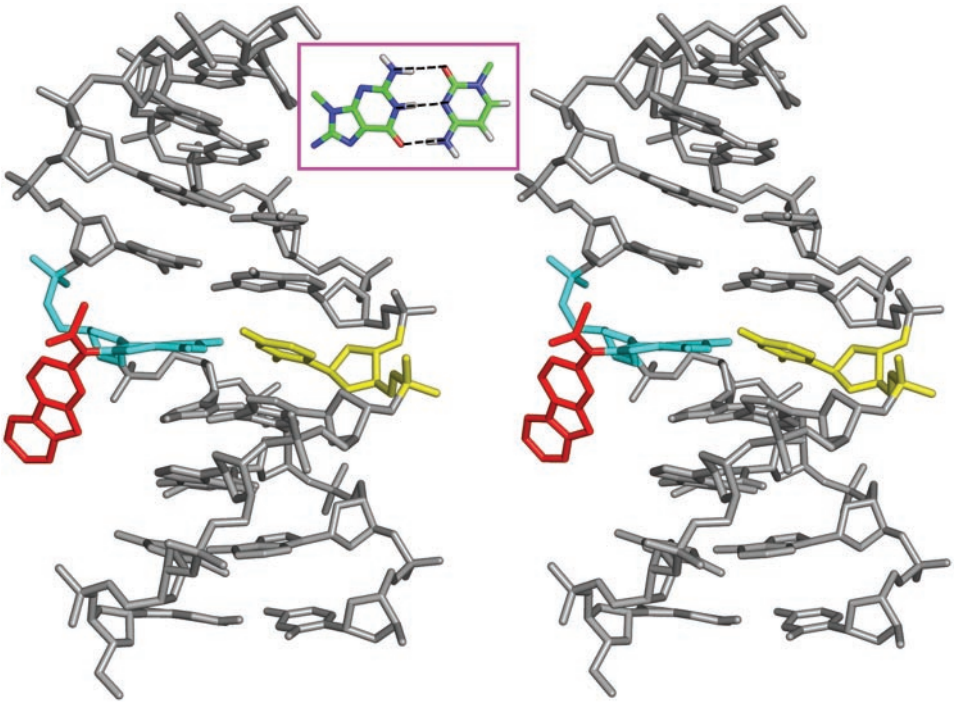

Figure 5. Stereoview of the *anti*-AAF-dG conformation in a duplex DNA. Inset shows the hydrogen bonding scheme of AAF-dG. Color code: AAF, red; modified dG, cyan; partner dC, yellow.

may also be feasible on the duplex level. One may hypothesize, by analogy to the AF-dG structures (11), that neighboring sequence context may influence the population balance between the *anti* major groove and *syn* base-displaced intercalated conformational families. This could explain chemical probing experiments for AAF-dG in the *Nar*I sequence (5′-$G_1G_2CG_3CC$-3′), which showed different conformers depending upon which G is modified (44). Belguise-Valladier and Fuchs (44) have proposed that 'the polymorphism in adduct-induced DNA structure . . . plays a major role in the sequence-specific responses seen when these lesions are processed *in vivo*'. We would also suggest that the differential processing of AF-dG and AAF-dG by replicative and repair enzymes originates in the differences in population balance between the two states in the pair of adducts. Studies with benzo[*a*]pyrene-derived DNA adducts have shown that base-displaced intercalated conformers are highly excised (78).

CONCLUSION

Our simulations showed that *anti*-AAF-dG can be harbored at the Dpo4 active site via a C1′-*exo* puckered sugar conformation, with the acetyl group oriented 5′, and the fluorenyl moiety directed 3′ to the modified strand. This conformation can readily accommodate an incoming dCTP with W/C base pairing and scarcely distorts the active site. Other nucleotides are less favored. This is consistent with the preferential incorporation of dC opposite AAF-dG in Dpo4 (26), and may also be relevant to this preference in a number of other polymerases (27–30,32). The predominant blockage one base prior to and opposite the lesion, observed even in Dpo4, could be explained by the distorting nature of the AAF-dG's preferred *syn* conformation, and the hindrance to the subsequent little finger translocation/dNTP binding following dNTP incorporation opposite *anti*-AAF-dG. Nucleotide incorporation (preferably dCTP) opposite AAF-dG is a common intermediate step for translesion synthesis, whether through slipped or non-slipped pathways (35,79); the sequence context determines whether slippage will occur (23,33–38). The *anti*-AAF-dG conformer found in our simulations may be a possible common intermediate in slipped and non-slipped pathways.

SUPPLEMENTARY DATA

Supplementary Data are available at NAR Online.

ACKNOWLEDGEMENTS

We thank Professor Robert Shapiro for his critical reading of the manuscript and very thoughtful insights. This work is supported by NIH Grant CA 2R01 CA75449 to SB. Funding to pay the Open Access publication charges for this article was provided by NIH grant CA75449.

Conflict of interest statement. None declared.

REFERENCES

1. Heflich,R.H. and Neft,R.E. (1994) Genetic toxicity of 2-acetylaminofluorene, 2-aminofluorene and some of their metabolites and model metabolites. *Mutat. Res.*, **318**, 73–114.

2. Kriek,E. (1992) Fifty years of research on *N*-acetyl-2-aminofluorene, one of the most versatile compounds in experimental cancer research. *J. Cancer Res. Clin. Oncol.*, **118**, 481–489.
3. Kriek,E. (1972) Persistent binding of a new reaction product of the carcinogen *N*-hydroxy-*N*-2-acetylaminofluorene with guanine in rat liver DNA *in vivo*. *Cancer Res.*, **32**, 2042–2048.
4. Fuchs,R.P. (1978) Arylamidation and arylation by the carcinogen *N*-2-fluorenylacetamide: a sensitive and rapid radiochemical assay. *Anal. Biochem.*, **91**, 663–673.
5. Grunberger,D., Nelson,J.H., Cantor,C.R. and Weinstein,I.B. (1970) Coding and conformational properties of oligonucleotides modified with the carcinogen *N*-2-acetylaminofluorene. *Proc. Natl Acad. Sci. USA*, **66**, 488–494.
6. Fuchs,R. and Daune,M. (1971) Changes of stability and conformation of DNA following the covalent binding of a carcinogen. *FEBS Lett.*, **14**, 206–208.
7. Fuchs,R. and Daune,M. (1972) Physical studies on deoxyribonucleic acid after covalent binding of a carcinogen. *Biochemistry*, **11**, 2659–2666.
8. Evans,F.E., Miller,D.W. and Beland,F.A. (1980) Sensitivity of the conformation of deoxyguanosine to binding at the C-8 position by *N*-acetylated and unacetylated 2-aminofluorene. *Carcinogenesis*, **1**, 955–959.
9. O'Handley,S.F., Sanford,D.G., Xu,R., Lester,C.C., Hingerty,B.E., Broyde,S. and Krugh,T.R. (1993) Structural characterization of an *N*-acetyl-2-aminofluorene (AAF) modified DNA oligomer by NMR, energy minimization, and molecular dynamics. *Biochemistry*, **32**, 2481–2497.
10. Milhe,C., Dhalluin,C., Fuchs,R.P. and Lefevre,J.F. (1994) NMR evidence of the stabilisation by the carcinogen *N*-2-acetylaminofluorene of a frameshift mutagenesis intermediate. *Nucleic Acids Res.*, **22**, 4646–4652.
11. Patel,D.J., Mao,B., Gu,Z., Hingerty,B.E., Gorin,A., Basu,A.K. and Broyde,S. (1998) Nuclear magnetic resonance solution structures of covalent aromatic amine-DNA adducts and their mutagenic relevance. *Chem. Res. Toxicol.*, **11**, 391–407.
12. Cho,B.P. (2004) Dynamic conformational heterogeneities of carcinogen-DNA adducts and their mutagenic relevance. *J. Environ. Sci. Health C Environ. Carcinog. Ecotoxicol. Rev.*, **22**, 57–90.
13. Cho,B.P., Beland,F.A. and Marques,M.M. (1994) NMR structural studies of a 15-mer DNA duplex from a *ras* protooncogene modified with the carcinogen 2-aminofluorene: conformational heterogeneity. *Biochemistry*, **33**, 1373–1384.
14. Mao,B., Gorin,A., Gu,Z., Hingerty,B.E., Broyde,S. and Patel,D.J. (1997) Solution structure of the aminofluorene-intercalated conformer of the *syn* [AF]-C^8-dG adduct opposite a -2 deletion site in the *Nar*I hot spot sequence context. *Biochemistry*, **36**, 14479–14490.
15. Mao,B., Gu,Z., Gorin,A., Hingerty,B.E., Broyde,S. and Patel,D.J. (1997) Solution structure of the aminofluorene-stacked conformer of the *syn* [AF]-C^8-dG adduct positioned at a template-primer junction. *Biochemistry*, **36**, 14491–14501.
16. Mao,B., Hingerty,B.E., Broyde,S. and Patel,D.J. (1998) Solution structure of the aminofluorene [AF]-external conformer of the *anti*-[AF]-C^8-dG adduct opposite dC in a DNA duplex. *Biochemistry*, **37**, 95–106.
17. Mao,B., Hingerty,B.E., Broyde,S. and Patel,D.J. (1998) Solution structure of the aminofluorene [AF]-intercalated conformer of the *syn*-[AF]-C^8-dG adduct opposite dC in a DNA duplex. *Biochemistry*, **37**, 81–94.
18. Broyde,S. and Hingerty,B. (1983) Conformation of 2-aminofluorene-modified DNA. *Biopolymers*, **22**, 2423–2441.
19. Hingerty,B. and Broyde,S. (1982) Conformation of the deoxydinucleoside monophosphate dCpdG modified at carbon 8 of guanine with 2-(acetylamino)fluorene. *Biochemistry*, **21**, 3243–3252.
20. Shapiro,R., Sidawi,D., Miao,Y.S., Hingerty,B.E., Schmidt,K.E., Moskowitz,J. and Broyde,S. (1994) Conformation of amine-modified DNA: 2-aminofluorene- and 2-(acetylamino)fluorene-modified deoxydinucleoside monophosphates with all possible nearest neighbors. A comparison of search and optimization methods. *Chem. Res. Toxicol.*, **7**, 239–253.
21. Hsu,G.W., Kiefer,J.R., Burnouf,D., Becherel,O.J., Fuchs,R.P. and Beese,L.S. (2004) Observing translesion synthesis of an aromatic amine DNA adduct by a high-fidelity DNA polymerase. *J. Biol. Chem.*, **279**, 50280–50285.
22. Lindsley,J.E. and Fuchs,R.P. (1994) Use of single-turnover kinetics to study bulky adduct bypass by T7 DNA polymerase. *Biochemistry*, **33**, 764–772.
23. Shibutani,S. and Grollman,A.P. (1993) On the mechanism of frameshift (deletion) mutagenesis *in vitro*. *J. Biol. Chem.*, **268**, 11703–11710.
24. Shibutani,S., Suzuki,N. and Grollman,A.P. (1998) Mutagenic specificity of (acetylamino)fluorene-derived DNA adducts in mammalian cells. *Biochemistry*, **37**, 12034–12041.
25. Suzuki,N., Ohashi,E., Hayashi,K., Ohmori,H., Grollman,A.P. and Shibutani,S. (2001) Translesional synthesis past acetylaminofluorene-derived DNA adducts catalyzed by human DNA polymerase kappa and *Escherichia coli* DNA polymerase IV. *Biochemistry*, **40**, 15176–15183.
26. Boudsocq,F., Iwai,S., Hanaoka,F. and Woodgate,R. (2001) *Sulfolobus solfataricus* P2 DNA polymerase IV (Dpo4): an archaeal DinB-like DNA polymerase with lesion-bypass properties akin to eukaryotic polη. *Nucleic Acids Res.*, **29**, 4607–4616.
27. Zhang,Y., Yuan,F., Wu,X., Taylor,J.S. and Wang,Z. (2001) Response of human DNA polymerase iota to DNA lesions. *Nucleic Acids Res.*, **29**, 928–935.
28. Masutani,C., Kusumoto,R., Iwai,S. and Hanaoka,F. (2000) Mechanisms of accurate translesion synthesis by human DNA polymerase η. *EMBO J.*, **19**, 3100–3109.
29. Rabkin,S.D. and Strauss,B.S. (1984) A role for DNA polymerase in the specificity of nucleotide incorporation opposite *N*-acetyl-2-aminofluorene adducts. *J. Mol. Biol.*, **178**, 569–594.
30. Yuan,F., Zhang,Y., Rajpal,D.K., Wu,X., Guo,D., Wang,M., Taylor,J.S. and Wang,Z. (2000) Specificity of DNA lesion bypass by the yeast DNA polymerase η. *J. Biol. Chem.*, **275**, 8233–8239.
31. Belguise-Valladier,P., Maki,H., Sekiguchi,M. and Fuchs,R.P. (1994) Effect of single DNA lesions on *in vitro* replication with DNA polymerase III holoenzyme. Comparison with other polymerases. *J. Mol. Biol.*, **236**, 151–164.
32. Yasui,M., Dong,H., Bonala,R.R., Suzuki,N., Ohmori,H., Hanaoka,F., Johnson,F., Grollman,A.P. and Shibutani,S. (2004) Mutagenic properties of 3-(deoxyguanosin-N^2-yl)-2-acetylaminofluorene, a persistent acetylaminofluorene-derived DNA adduct in mammalian cells. *Biochemistry*, **43**, 15005–15013.
33. Burnouf,D., Koehl,P. and Fuchs,R.P. (1989) Single adduct mutagenesis: strong effect of the position of a single acetylaminofluorene adduct within a mutation hot spot. *Proc. Natl Acad. Sci. USA*, **86**, 4147–4151.
34. Schaaper,R.M., Koffel-Schwartz,N. and Fuchs,R.P. (1990) *N*-acetoxy-*N*-acetyl-2-aminofluorene-induced mutagenesis in the *lacI* gene of *Escherichia coli*. *Carcinogenesis*, **11**, 1087–1095.
35. Shibutani,S., Suzuki,N. and Grollman,A.P. (2004) Mechanism of frameshift (deletion) generated by acetylaminofluorene-derived DNA adducts *in vitro*. *Biochemistry*, **43**, 15929–15935.
36. Thomas,D.C., Veaute,X., Fuchs,R.P. and Kunkel,T.A. (1995) Frequency and fidelity of translesion synthesis of site-specific *N*-2-acetylaminofluorene adducts during DNA replication in a human cell extract. *J. Biol. Chem.*, **270**, 21226–21233.
37. Thomas,D.C., Veaute,X., Kunkel,T.A. and Fuchs,R.P. (1994) Mutagenic replication in human cell extracts of DNA containing site-specific *N*-2-acetylaminofluorene adducts. *Proc. Natl Acad. Sci. USA*, **91**, 7752–7756.
38. Gill,J.P. and Romano,L.J. (2005) Mechanism for *N*-acetyl-2-aminofluorene-induced frameshift mutagenesis by *Escherichia coli* DNA polymerase I (Klenow fragment). *Biochemistry*, **44**, 15387–15395.
39. Nair,D.T., Johnson,R.E., Prakash,L., Prakash,S. and Aggarwal,A.K. (2005) Human DNA polymerase iota Incorporates dCTP opposite template G via a G.C+ Hoogsteen base pair. *Structure*, **13**, 1569–1577.
40. Nair,D.T., Johnson,R.E., Prakash,S., Prakash,L. and Aggarwal,A.K. (2004) Replication by human DNA polymerase iota occurs by Hoogsteen base-pairing. *Nature*, **430**, 377–380.
41. Nair,D.T., Johnson,R.E., Prakash,L., Prakash,S. and Aggarwal,A.K. (2005) Rev1 employs a novel mechanism of DNA synthesis using a protein template. *Science*, **309**, 2219–2222.
42. Ling,H., Boudsocq,F., Woodgate,R. and Yang,W. (2001) Crystal structure of a Y-family DNA polymerase in action: a mechanism for error-prone and lesion-bypass replication. *Cell*, **107**, 91–102.
43. Vaisman,A., Ling,H., Woodgate,R. and Yang,W. (2005) Fidelity of Dpo4: effect of metal ions, nucleotide selection and pyrophosphorolysis. *EMBO J.*, **24**, 2957–2967.

44. Belguise-Valladier,P. and Fuchs,R.P. (1991) Strong sequence-dependent polymorphism in adduct-induced DNA structure: analysis of single *N*-2-acetylaminofluorene residues bound within the *Nar*I mutation hot spot. *Biochemistry*, **30**, 10091–10100.
45. Ling,H., Sayer,J.M., Plosky,B.S., Yagi,H., Boudsocq,F., Woodgate,R., Jerina,D.M. and Yang,W. (2004) Crystal structure of a benzo[*a*]pyrene diol epoxide adduct in a ternary complex with a DNA polymerase. *Proc. Natl Acad. Sci. USA*, **101**, 2265–2269.
46. Berman,H.M., Westbrook,J., Feng,Z., Gilliland,G., Bhat,T.N., Weissig,H., Shindyalov,I.N. and Bourne,P.E. (2000) The Protein Data Bank. *Nucleic Acids Res.*, **28**, 235–242.
47. van Meerssche,M., Germain,G., Declercq,J.-P., Touillaux,R., Roberfroid,M. and Razzouk,C. (1980) 2-(Acetylamino)fluorene, $C_{15}H_{13}NO$. *Acta Crystallogr. C Cryst. Struct. Commun.*, **9**, 515–518.
48. Ling,H., Boudsocq,F., Plosky,B.S., Woodgate,R. and Yang,W. (2003) Replication of a *cis-syn* thymine dimer at atomic resolution. *Nature*, **424**, 1083–1087.
49. Duan,Y., Wu,C., Chowdhury,S., Lee,M.C., Xiong,G., Zhang,W., Yang,R., Cieplak,P., Luo,R. and Lee,T. (2003) A point-charge force field for molecular mechanics simulations of proteins. *J. Comput. Chem.*, **24**, 1999–2012.
50. Cornell,W.D., Cieplak,P., Bayly,C.I., Gould,I.R., Merz,K.M., Ferguson,D.M., Spellmeyer,D.C., Fox,T., Caldwell,J.W. and Kollman,P.A. (1995) A second generation force field for the simulation of proteins, nucleic acids, and organic molecules. *J. Am. Chem. Soc.*, **117**, 5179–5197.
51. Cheatham,T.E.,III, Cieplak,P. and Kollman,P.A. (1999) A modified version of the Cornell *et al*. force field with improved sugar pucker phases and helical repeat. *J. Biomol. Struct. Dyn.*, **16**, 845–862.
52. Jorgensen,W.L., Chandrasekhar,J., Madura,J. and Klein,M.L. (1983) Comparison of simple potential functions for simulating liquid water. *J. Chem. Phys.*, **79**, 926–935.
53. Darden,T., York,D. and Pedersen,L. (1993) Particle mesh Ewald: an N×log(N) method for Ewald sums in large systems. *J. Chem. Phys.*, **98**, 10089–10092.
54. Essmann,U., Perera,L., Berkowitz,M.L., Darden,T., Lee,H. and Pedersen,L.G. (1995) A smooth particle mesh Ewald method. *J. Chem. Phys.*, **103**, 8577–8593.
55. Ryckaert,J.-P., Ciccotti,G. and Berendsen,H.J.C. (1977) Numerical integration of the cartesian equations of motion of a system with constraints: molecular dynamics of *n*-alkanes. *J. Comput. Phys.*, **23**, 327–341.
56. Berendsen,H.J.C., Postma,J.P.M., van Gunsteren,W.F., DiNola,A. and Haak,J.R. (1984) Molecular dynamics with coupling to an external bath. *J. Chem. Phys.*, **81**, 3684–3690.
57. Harvey,S.C., Tan,R.K.Z. and Cheatham,T.E.,III (1998) The flying ice cube: velocity rescaling in molecular dynamics leads to violation of energy equipartition. *J. Comput. Chem.*, **19**, 726–740.
58. Bayly,C.I., Cieplak,P., Cornell,W.D. and Kollman,P.A. (1993) A well-behaved electrostatic potential based method using charge restraints for deriving atomic charges—the RESP model. *J. Phys. Chem.*, **97**, 10269–10280.
59. Wang,J.M., Cieplak,P. and Kollman,P.A. (2000) How well does a restrained electrostatic potential (RESP) model perform in calculating conformational energies of organic and biological molecules? *J. Comp. Chem.*, **21**, 1049–1074.
60. Perlow,R.A. and Broyde,S. (2001) Evading the proofreading machinery of a replicative DNA polymerase: induction of a mutation by an environmental carcinogen. *J. Mol. Biol.*, **309**, 519–536.
61. Perlow,R.A. and Broyde,S. (2002) Toward understanding the mutagenicity of an environmental carcinogen: structural insights into nucleotide incorporation preferences. *J. Mol. Biol.*, **322**, 291–309.
62. Altona,C. and Sundaralingam,M. (1972) Conformational analysis of the sugar ring in nucleosides and nucleotides. A new description using the concept of pseudorotation. *J. Am. Chem. Soc.*, **94**, 8205–8212.
63. Berman,H.M., Olson,W.K., Beveridge,D.L., Westbrook,J., Gelbin,A., Demeny,T., Hsieh,S.H., Srinivasan,A.R. and Schneider,B. (1992) The nucleic acid database. A comprehensive relational database of three-dimensional structures of nucleic acids. *Biophys. J.*, **63**, 751–759.
64. Barsky,D., Kool,E.T. and Colvin,M.E. (1999) Interaction and solvation energies of nonpolar DNA base analogues and their role in polymerase insertion fidelity. *J. Biomol. Struct. Dyn.*, **16**, 1119–1134.
65. Kool,E.T. (2002) Active site tightness and substrate fit in DNA replication. *Annu. Rev. Biochem.*, **71**, 191–219.
66. Jordan,F. (1973) Lennard-Jones potential calculations of the barrier to rotation around the glycosidic C-N linkage in selected purine nucleosides and nucleotides. A direct comparison of the results of 6-12 potential calculations with results of semiempirical molecular orbital studies. *J. Theor. Biol.*, **41**, 375–395.
67. Brautigam,C.A. and Steitz,T.A. (1998) Structural and functional insights provided by crystal structures of DNA polymerases and their substrate complexes. *Curr. Opin. Struct. Biol.*, **8**, 54–63.
68. Berman,H.M. (1997) Crystal studies of B-DNA: the answers and the questions. *Biopolymers*, **44**, 23–44.
69. Dutta,S., Li,Y., Johnson,D., Dzantiev,L., Richardson,C.C., Romano,L.J. and Ellenberger,T. (2004) Crystal structures of 2-acetylaminofluorene and 2-aminofluorene in complex with T7 DNA polymerase reveal mechanisms of mutagenesis. *Proc. Natl Acad. Sci. USA*, **101**, 16186–16191.
70. Pages,V. and Fuchs,R.P. (2002) How DNA lesions are turned into mutations within cells? *Oncogene*, **21**, 8957–8966.
71. Prakash,S., Johnson,R.E. and Prakash,L. (2005) Eukaryotic translesion synthesis DNA polymerases: specificity of structure and function. *Annu. Rev. Biochem.*, **74**, 317–353.
72. Ling,H., Boudsocq,F., Woodgate,R. and Yang,W. (2004) Snapshots of replication through an abasic lesion; structural basis for base substitutions and frameshifts. *Mol. Cell*, **13**, 751–762.
73. Rechkoblit,O., Malinina,L., Cheng,Y., Kuryavyi,V., Broyde,S., Geacintov,N.E. and Patel,D.J. (2006) Stepwise translocation of Dpo4 polymerase during error-free bypass of an oxoG lesion. *PLoS Biol.*, **4**, e11.
74. Kunkel,T.A. and Alexander,P.S. (1986) The base substitution fidelity of eucaryotic DNA polymerases. Mispairing frequencies, site preferences, insertion preferences, and base substitution by dislocation. *J. Biol. Chem.*, **261**, 160–166.
75. Gillet,L.C., Alzeer,J. and Scharer,O.D. (2005) Site-specific incorporation of *N*-(deoxyguanosin-8-yl)-2-acetylaminofluorene (dG-AAF) into oligonucleotides using modified 'ultra-mild' DNA synthesis. *Nucleic Acids Res.*, **33**, 1961–1969.
76. Shui,X., McFail-Isom,L., Hu,G.G. and Williams,L.D. (1998) The B-DNA dodecamer at high resolution reveals a spine of water on sodium. *Biochemistry*, **37**, 8341–8355.
77. Wang,L., Hingerty,B.E., Srinivasan,A.R., Olson,W.K. and Broyde,S. (2002) Accurate representation of B-DNA double helical structure with implicit solvent and counterions. *Biophys. J.*, **83**, 382–406.
78. Hess,M.T., Gunz,D., Luneva,N., Geacintov,N.E. and Naegeli,H. (1997) Base pair conformation-dependent excision of benzo[*a*]pyrene diol epoxide-guanine adducts by human nucleotide excision repair enzymes. *Mol. Cell. Biol.*, **17**, 7069–7076.
79. Baynton,K., Bresson-Roy,A. and Fuchs,R.P. (1999) Distinct roles for Rev1p and Rev7p during translesion synthesis in *Saccharomyces cerevisiae*. *Mol. Microbiol.*, **34**, 124–133.
80. Saenger,W. (1984) Sugar puckering modes: the pseudorotation cycle. In Cantor,C.R. (ed.), *Principles of Nucleic Acid Structure*. Springer-Verlag, NY, pp. 17–21.